A high-resolution version of the WRF (Weather Research and Forecasting) model has been used to study the fine structure of a cloud head and its associated cold conveyor belt jet (CJ) and sting jet (SJ) in an intense extratropical cyclone that produced damaging surface winds in northern Ireland and central Scotland on 3 January 2012. The model was run with many different initialisation times and physical parametrisations, and a run was selected that verified well against a variety of observations. New methods have been devised to visualise the 3D structure of the CJ and SJ and to attribute strong surface winds to one or other of them, and the validity of regarding the SJ as a semi-Lagrangian feature has been assessed. The model suggests that, whereas the CJ remained mainly below the 850 hPa level as it circulated around the bent-back front, the SJ consisted of a stream or streams of air within the bent-back frontal zone that first ascended from close to the surface into the middle and upper-level parts of the cloud head before descending from evaporating cloud filaments at the tip of the cloud head and reaching the top of the boundary layer slightly ahead of the CJ. The simulations did not support the idea that either the evaporation or conditional symmetric instability (CSI) played a major role in the development of these jets. The strong gusts (up to 47 m s^{-1}) which were recorded on the north coast of Ireland appear to have been due mainly to the CJ, which by then was undercutting the SJ. The SJ was responsible for stronger surface winds than the CJ several hours earlier during the initial stage of frontal fracture, but only for a limited period.

Key Words: extratropical cyclone; damaging winds; frontal fracture; bent-back front; WRF; mesoscale model

Received 22 October 2012; Revised 22 February 2013; Accepted 27 March 2013; Published online in Wiley Online Library

Citation: Smart DJ, Browning KA. 2013. Attribution of strong winds to a cold conveyor belt and sting jet. *Q. J. R. Meteorol. Soc.* DOI:10.1002/qj.2162

1. Introduction

It has long been recognised that there is a certain kind of extratropical cyclone that is liable to produce the most damaging winds. This is a cyclone that goes through a process of frontal fracture leading to the formation of a bent-back front (BBF; Shapiro and Keyser, 1990; Neimann *et al.*, 1993). Norwegian meteorologists were the first to realise that the strongest winds tend to occur in association with the BBF which they referred to as 'the poisonous tail' (Grønås, 1995). The winds there tend to reach their peak when the cyclone is close to attaining its lowest central pressure. This often follows a period of sustained and rapid development: deepening by 24 hPa or more in 24 hours may

airstream with an upper-level jet streak reaching almost $90\ \mathrm{m\ s^{-1}}$

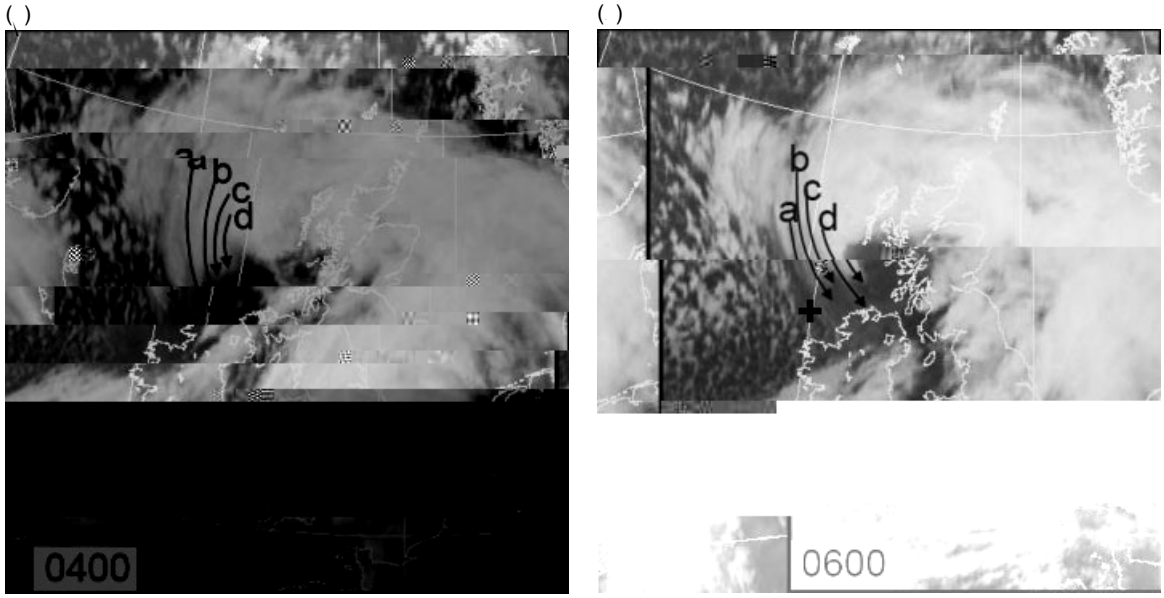

Figure 1. MSG (MeteoSat Geostationary) IR imagery at (a) 0400 UTC, (b) 0600 UTC on 3 January 2012. Four cloud filaments a, b, c, d are indicated by the labelled arrows (derived from examination of 15 min imagery). (Courtesy and copyright EUMETSAT/UKMO). The location of Malin Head is marked by a +.

the WRF (Weather Research and Forecasting) model to investigate the evolving 3D structure of the CJ and SJ in this storm, and thereby clarify their relationship to one another and, as far as possible (given the possible limitations of the model in, for example, representing the effects of latent cooling), determine which kind of jets were likely to have been responsible for the strongest surface winds during and before the period when it was affecting the north of Ireland. This period was chosen because it included some of the strongest surface winds and because much of the system was over the sea and relatively uninfluenced by topographical effects which did not appear to be well represented by the model.

The article is structured as follows. In section 2, the configuration of the WRF model is described, together with the reasons for selecting a particular run, initialised as much as 3 days before the storm arrived. In section 3, the chosen run is evaluated against a variety of observational sources. We believe that the credibility of our study owes a lot to the painstaking validation of the model against observations and the selection of the best performing model run from a variety of runs not only initialised at different times but also using different combinations of parametrisation schemes. Model diagnostics showing the 3D structure of the jets are given in section 4.1 for a time during the mature frontal fracture phase of the storm before it made landfall. The evolution of the footprint of strong surface winds and their attribution to the CJ and SJ are presented in section 4.2. A general discussion and conclusions are given in section 5.

2. The model

-

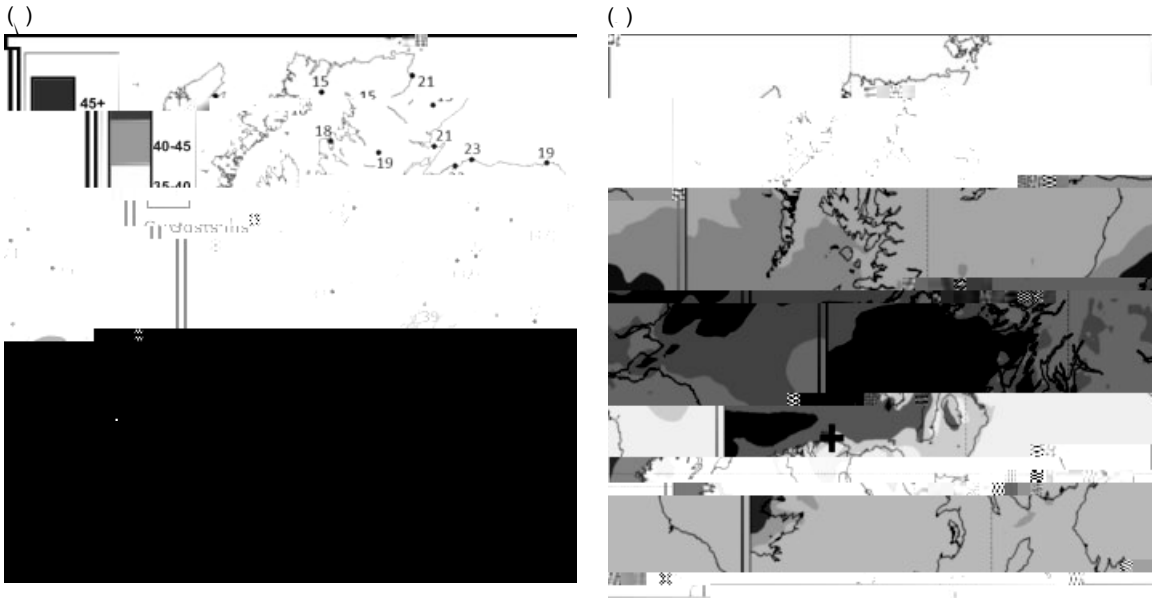

Figure 4. Comparison of time-integrated observed and modelled 10-m gust footprints. (a) Maximum surface gust observations ($\mathrm{m\,s^{-1}}$) from weather stations, 0300–1200 UTC on 3 January 2012. Values from stations with elevations above 400 m are in brackets. The gust magnitude for Malin Head is shown in white. Manually interpolated gust contours, ignoring the bracketed values, are shaded according to inset key. (The original figure was kindly prepared by Matthew Clark from Met Office data, by courtesy of and copyright UKMO). (b) Time-integrated diagnosed maximum 10 m wind gusts ($\mathrm{m\,s^{-1}}$), 0300–1200 UTC on 3 January (shaded as in (a)) from model Domain 2. The location of Malin Head is marked by a +.

because there are maxima in the surface wind gust footprint attributable to SJs which are distinct from the maximum due to the CJ at this time. We shall show evidence for a causal relationship between the individual jets and particular parts of the footprint of strong surface wind gusts. Figure 5 shows the structure of the BBF and frontal fracture regions at or close to the surface at 0300 UTC. We have labelled local wind speed maxima within the footprint of surface wind gusts according to whether they are shown to be due to the CJ or to one of two separate SJs: the sting jet labelled SJ2 corresponds, as we shall demonstrate, to the main SJ at this time and that labelled SJ1 corresponds to the remains of one that had been the main SJ at earlier times. Figure 5 shows that the two maxima labelled SJ1 and SJ2 are associated with θ_w values at 950 hPa, corresponding to a level only 200 m above the surface, of around 9.5 and 8.5 °C, respectively; the wind maximum labelled CJ is associated with a much lower value for θ_w of 6–7 °C.

In order to analyse the structure of the BBF and associated CJ and SJ, we have manually constructed a number of transverse sections along radials, at roughly 20° intervals, approximately normal to the BBF and radiating from the manually determined centroid of the arc formed by the BBF. This is a novel feature of the analysis which we

travel the full length of the jet axis, all the way from 520 to 800 hPa: they do not. As we shall see, trajectory analyses show that individual air parcels descend down only portions of the jet axis.)

The axis of the entire SJ2 starts from a position 70 km to the left (i.e. to the west) of the CJ in section A and reaches a position directly above the CJ between sections D and E. By the time the CJ reaches section E, the only evidence of the CJ is a weakening velocity maximum associated with air of slightly higher θ_w at its leading edge: the leading edge of the CJ air with θ_w of 6 °C lies somewhere between D and E. Finally, in section F, the CJ is seen to be totally absent and the dominant low-level jet, at 800 hPa, is SJ2 with a θ_w of 8 °C. The other sting jet, SJ1, can also be seen in section F: it has a slightly higher velocity than SJ2 but is higher up, with a higher θ_w of about 9 °C. As noted above and discussed later, SJ1 is responsible for the local maximum in the surface gust footprint labelled SJ1 in Figure 5, just ahead of the surface gust maximum due to SJ2. There is no evidence of SJ1 in any of the other sections in Figure 6(a–e), the portion of SJ1 in section F (Figure 6(f)) being just the remnant of the jet that had dominated during the preceding 3 h. We shall be focussing our attention mainly on SJ2 in this subsection.

To show the nature of the SJ more clearly, we employ the technique of analysing the model fields on moist isentropic surfaces (Figures 7(a, b)). The moist isentropic framework (e.g. Browning and Harrold, 1969) assumes that the flows are essentially confined to and conserved along moist isentropic (i.e. constant θ_w) surfaces assuming minimal mixing and essentially moist adiabatic processes. We demonstrate later that this is a good approximation for air parcels in the SJ. It is a poorer assumption for the CJ but the conclusions we draw from the corresponding analysis are thought to be broadly correct. Figure 7(a) gives the analysis for the 6 °C θ_w surface to represent the CJ (the axis of which is shown by the dashed arrow) and Figure 7(b) shows the corresponding analysis for the 8.5 °C surface to represent SJ2 (the bold, solid arrow). Figure 7(a) shows the CJ remaining within saturated or almost saturated air in the lower part of the cloud head with very little significant change of height in time, whereas the strongly sloping axis of SJ2 can be seen originating within the saturated air of the cloud head (white shading) and then emerging from it. The rate of advance of the leading edge of the cloud head is slower, by as much as 17 m s^{-1}, than the velocity of the air in SJ2, which is symptomatic of the ongoing evaporation of the tip of the cloud head in this region of descending flow. The descending air in SJ2 undergoes strong divergence as it nears the surface and this leads to the widening of the gap between the 8 and 9 °C θ_w contours at 950 hPa that was evident in Figure 5; this is, of course, all part of the process of frontal fracture.

Figure 8 summarises the disposition of the principal jets as analysed in Figures 5–7. Both the CJ and the SJ are seen to curve around the cloud head. The CJ remains centred close to 900 hPa whilst the SJ descends from 520 to 800 hPa. The two jets originate from different parts of the cloud head but, by the time they reach the position of section D, they are close together in plan view, almost one above the other

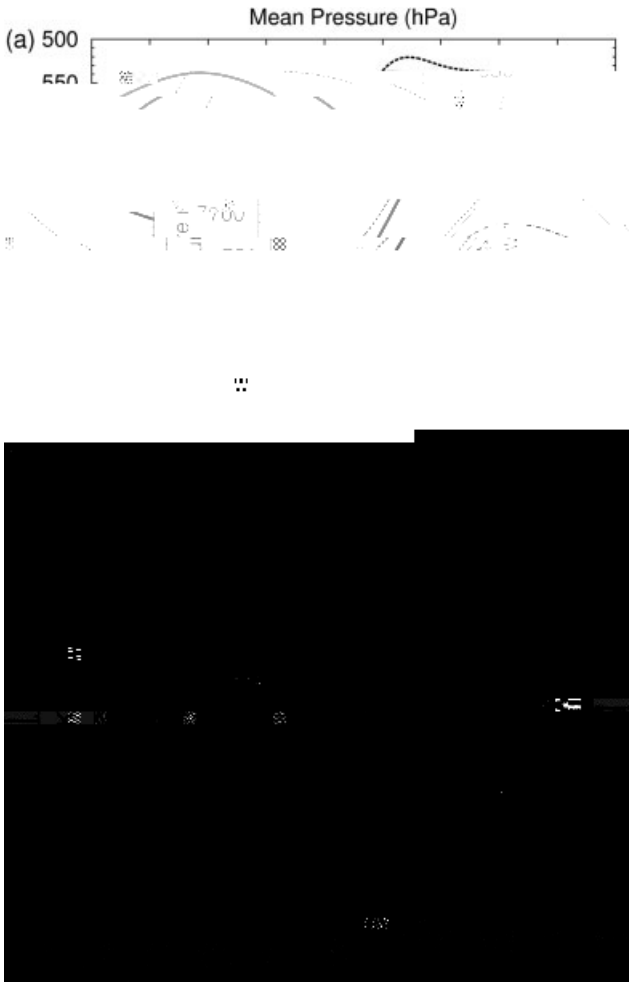

Figure 10. Mean properties of trajectory parcels initialised in the SJ2 core at cross-sections A (A–A′) to F (F–F′): (a) mean pressure (hPa), and (b) mean θ (K). Time is in model hours (UTC).

model is capable of properly representing the evaporative cooling, this would suggest that this was not an important mechanism for the SJ in this storm. However, there is evidence (not shown), of a decrease in potential temperature of up to 3 K for parcels initiated 50 hPa below the core of the SJ once the SJ had descended below 700 hPa. It appears that this is due partly to evaporation of cloud in the moist layer immediately beneath the SJ, perhaps due to mixing with the overlying dry air from the core of the SJ. Such mixing would also account for the decrease in θ_w seen in the last section (F) in Table 2, but it also means that some of the decrease in (dry bulb) potential temperature (θ) in section F would also be a direct consequence of mixing with the cooler air below rather than being entirely due to evaporation associated with the mixing.

We shall now clarify the location of a SJ parcel within the bent-back frontal zone as it first ascended and then descended. We focus again on the parcel showing the greatest vertical excursion, the diagnostics for which were plotted in Figure 9. Figure 11 shows the plan position of this SJ2 parcel with respect to the frontal zone at effectively hourly intervals during this cycle. The four panels in Figure 11 are actually for (a) 1900, (b) 2200, (c) 0100 and (d) 0400 UTC, but for each panel we have plotted the system-relative positions of the parcel at ± 1 h (open circles) as well as the position at the map time (solid black circles). Figure 11(a) shows the parcel at 1800, 1900 and 2000 UTC on 2 January just before it started to ascend, during which time it had an earth-relative speed of 19 m s^{-1} and was close to the lowest model layer, i.e. close to the relatively warm sea surface. Figure 11(b) shows it at 2100, 2200 and 2300 UTC, having risen to the 650 hPa level by 2200 UTC, with a wind speed of only 8 m s^{-1}. Figure 11(c) shows it at 0000, 0100 and 0200 UTC on 3 January, at the end of its main period of ascent; by 0100 UTC it had reached the 520 hPa level. Figure 11(d) shows the parcel at 0300, 0400 and 0500 UTC during its main period of descent and increasing speed within the evaporating cloud head; at 0400 UTC it was at 610 hPa and by 0500 UTC it had reached the 670 hPa level, with a speed of 45 m s^{-1}. It subsequently reached its lowest level (705 hPa) at 0530 UTC with a speed of 46 m s^{-1} (Figure 9 and Table 2). Throughout this 12 h cycle of ascent and descent, this and the other SJ parcels remained within the frontal zone. Their θ_w value of 8 to 8.5 °C from 2200 UTC onwards implies that

Table 2. Summary of properties of trajectory parcels initialised in the SJ2 core at cross-sections A (A–A′) to F (F–F′). In each case the values given here relate to the parcel initiated in the jet core at each section which exhibited the greatest descent rather than to the mean of the three parcels, although the difference is not large. Pressure values are rounded to the nearest 5 hPa, θ to the nearest 1 K, θ_w to 0.1 K and RH to the nearest 5%.

Trajectory set at cross-section:	A	B	C	D	E	F
Values at minimum pressure (*P*min)						
Time (UTC) on 3 January	0245	0100	0200	0130	0115	0100
Pressure (hPa)	480	520	610	650	710	700
Wind speed ($m\,s^{-1}$)	15	8	14	15	14	16
θ (K)	296	296	296	295	292	292
θ_w (°C)	8.5	8.5	8.4	8.5	8.0	8.5
Relative humidity (%)	100	100	100	105	100	100
Values at maximum pressure (*P*max)						
Time (UTC) on 3 January	0600	0530	0600	0430	0400	0400
Pressure (hPa)	650	705	760	770	800	820
Wind speed ($m\,s^{-1}$)	40	46	47	47	45	44
θ (K)	296	296	296	296	292	290
θ_w (°C)	8.3	8.3	8.2	8.4	7.8	8.0
Relative humidity (%)	40	20	30	20	50	60
*Difference between values at P*max *and P*min						
Time (h)	3.25	4.50	4.00	3.00	2.75	3.00
Pressure (hPa)	170	185	150	120	90	120
Wind speed ($m\,s^{-1}$)	35	38	33	32	31	28
θ (K)	0	0	0	1	0	−2
θ_w (C)	−0.2	−0.2	−0.2	−0.1	−0.2	−0.5
Relative humidity (%)	−60	−80	−70	−85	−50	−40

it was formed from air that had remained within the frontal zone while undergoing a cycle of ascent and descent over a 12 h period. The main acceleration occurred during the final 4 h period of descent towards the footprint of strong surface winds. The remains of another SJ, referred to as SJ1, contributed to another part of the footprint of strong surface winds and is discussed in section 4.2.

4.2. The evolving footprint of strong surface winds

We conclude our analysis of the model storm by showing in Figure 12 the evolution of the footprint of strong surface wind gusts and the pattern of θ_w at 950 hPa (i.e. within 200 m of the surface) during the process of frontal fracture and seclusion. The hourly plots in Figure 12 are plotted in a frame of reference following the storm such that the low-pressure centre lies in the upper-central area of the plotting window. Frontal fracture can be seen to get under-way during the hours after 2000 UTC on 2 January (Figure 12(a)) and a warm seclusion begins to appear by 0400 UTC on 3 January (Figure 12(i)). A surface wind maximum due to the cold-conveyor-belt jet, CJ, forms on the cold side of the BBF at

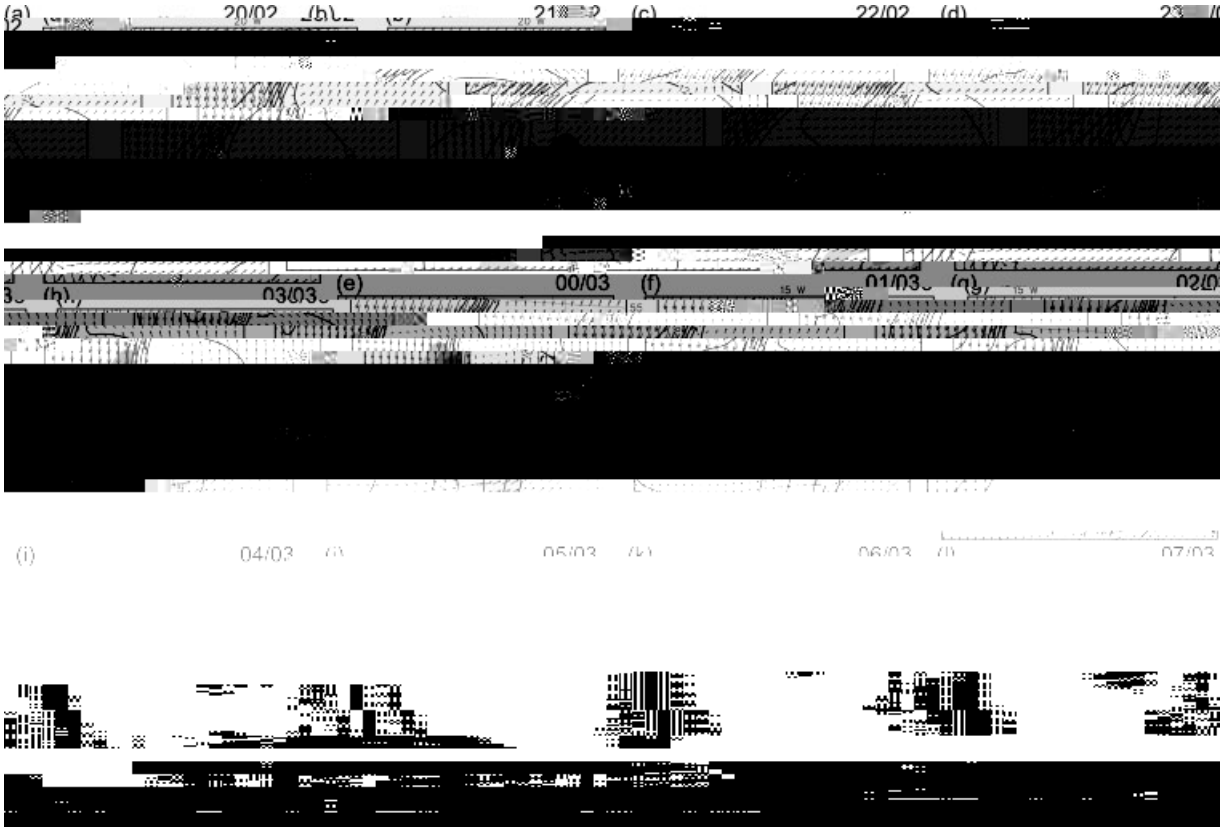

Figure 12. (a)–(l) The evolving footprint of strong surface winds plotted at 1 h intervals over a domain moving with the system, showing: 10 m wind gusts ($m\,s^{-1}$) shaded according to the key; θ_w at 950 hPa, contours every 1 °C; and system-relative flow vectors at 950 hPa. A system velocity of 17.9 $m\,s^{-1}$ from 210° is used throughout. The areas of strong surface winds attributed to the cold conveyor belt and sting jet, respectively, are labelled CJ and SJ in (f). The dashed line (in (f), (g) and (h) only and corresponding to the OLR 250 W m^{-2} contour) shows where the the descending SJ air has led to the total dissipation of the boundary-layer stratocumulus. The time (UTC)/day is given above the top right hand corner of each plot. Each plot is 300×250 km.

Table 3. Comparison of the properties of the lower edges of the CJ/**SJ** at 10 m above the surface. Figures for the **SJ** are in bold. Wind directions are estimated to the nearest 5°, and θ_w values to the nearest 0.5 °C. Divergence values are rounded to the nearest $5\times10^{-5}s^{-1}$.

Model time (UTC/day)	Maximum surface gust ($m\,s^{-1}$)	Wind direction at max. wind speed (° from north)	θ_w (°C)	Relative humidity (%)	Divergence ($10^{-5}s^{-1}$)
2100/02	30.2 / **30.8**	335 / **260**	6.5 / **11.0**	95 / **90**	0 / **0**
2200/02	31.5 / **32.9**	330 / **250**	6.5 / **11.0**	95 / **89**	0 / **5**
2300/02	33.6 / **34.1**	330 / **250**	6.5 / **10.5**	96 / **88**	0 / **5**
0000/03	35.2 / **36.8**	325 / **245**	7.0 / **10.0**	91 / **84**	5 / **10**
0100/03	38.5 / **37.8**	310 / **235**	7.0 / **10.0**	88 / **80**	10 / **15**
0200/03	45.1 / **38.1**	310 / **225**	8.0 / **9.5**	88 / **77**	10 / **30**

It was apparent from our 'ensemble' of different physics configurations (section 3) that the model near-surface fields were strongly dependent on the choice of microphysics, PBL and surface-layer parametrisation schemes. Although we have not discussed this in detail, analysis of the MYJ and MYNN runs (Table 1) produced quite different outcomes for the jets above and within the PBL (even though the resulting surface fields all appeared quite plausible). By comparing the model results with the Malin Head observations, we determined that the MYNN configuration produced results most nearly resembling the observed storm. The MYNN2 PBL module of this configuration, with its ability to predict greater vertical mixing than the MYJ scheme, was the likely key to this success.

Accurate prediction of the magnitude and areal extent of surface gusts is an important aspect of modelling severe extratropical cyclones for weather forecasting, climate change prediction and insurance risk assessment applications. The chosen MYNN run somewhat overpredicted wind gust strength in this case (Figure 3(a)) although 10 m mean winds were somewhat underpredicted. This may be because Malin Head, although on the coast, is still influenced signif-

icantly by the effect ofofinanmae8sTD8eessmJT*eD8eessm3TD4ig.48.2(ofcsempir.1(xT*[6-215e)]TJT*[(de687(this)-240.s632.1([6-253(

having a SJ, it does not necessarily follow that the strongest surface winds will always be associated with the SJ. It may well be the case that the strongest winds in some extremely severe storms, such as the October 1987 storm, are due to the SJ (Clark *et al.*, 2005), but further research is required to determine the factors responsible for the exceptional strength of the SJ in such cases.

Schultz (2001), in his study of a cold conveyor belt, draws attention to the fact that parcel trajectories do not necessarily follow the system-relative streamlines within a cold conveyor belt because of the crudeness of the steady-state assumption. The same is true for a SJ, but this is not necessarily inconsistent with parcels following the axis of a SJ as its shape changes over time. An important issue that we have addressed is the extent to which the SJ can be considered to be a semi-Lagrangian feature in which air parcels can be assumed to travel along the entire axis of the jet as observed at an instant in time. This was found to be so to only a first approximation. By starting clusters of trajectories (forwards and backwards) at a given time from six widely different locations along the axis of the SJ, which extended over a distance of 200 km and a pressure range of 280 hPa (from the 520 hPa level down to 800 hPa), we found that only one of these clusters descended by as much as 185 hPa. The others descended by between 170 and 90 hPa. This is probably due, at least in part, to the short lifetime of a given SJ. In this study we identified two separate SJs, one of which was sufficiently discrete that we were able to determine its lifetime. It was detectable for only 5 h. Moreover, during much of this time it was relatively weak and possibly less extensive in the vertical. Thus it appears likely that the SJ typically dissipates or diminishes in intensity before a given parcel has time to travel along its entire length.

The model output shows that the air parcels that formed the SJ ascended slantwise, parallel to the sloping frontal zone, into the cloud head, before descending within the evaporating tip of the cloud head. Schultz and Sienkiewicz (2013) suggest that the vertical motion of the SJ air is due to frontogenetic forcing, with the descending part of the trajectory corresponding to the region of frontolysis

in intense winter North-Atlantic windstorms. *Environ. Res. Lett.* **7**: 024014. DOI: 10.1088/1748-9326/7/2/024014

Nakanishi M, Niino H. 2004. An improved Mellor–Yamada level-3 model with condensation physics: Its design and verification. *Boundary-Layer Meteorol.* **112**: 1–31.

Neiman PJ, Shapiro MA, Fedor LS. 1993. The life cycle of an extratropical marine cyclone. Part II: Mesoscale structure and diagnostics. *Mon. Weather Rev.* **121**: 2177–2199.

Parton GA, Vaughan G, Norton EG, Browning KA, Clark PA. 2009. Wind profiler observations of a sting jet. *Q. J. R. Meteorol. Soc.* **135**: 663–680.

Sanders F, Gyakum JR. 1980. Synoptic-dynamic climatology of the 'Bomb'. *Mon. Weather Rev.* **108**: 1589–1606.

Schulz J-P. 2008. 'Revision of the turbulent gust diagnostics in the COSMO model'. *COSMO Newsletter* **8**: 17–22. Available at http://www.cosmo-model.org

Schultz DM. 2001. Re-examining the cold conveyor belt. *Mon. Weather Rev.* **129**: 2205–2225.

Schultz DM, Sienkiewicz JM. 2013. Using frontogenesis to identify sting jets in extratropical cyclones. *Weather Forecasting* in press. DOI: 10.1175/WAF-D-12-00126.1

Shapiro MA, Keyser D. 1990. Fronts, jet streams and the tropopause. In *Extratropical Cyclones: The Erik Palmén Memorial Volume*.